Fractional Shapiro steps in resistively shunted Josephson junctions as a fingerprint of a skewed current-phase relationship

B. Raes,[1,*] N. Tubsrinuan,[1,†] R. Sreedhar,[1,†] D. S. Guala,[1,†] R. Panghotra,[1] H. Dausy,[1]
Clécio C. de Souza Silva,[2] and J. Van de Vondel[1]

[1]*Quantum Solid-State Physics, Department of Physics and Astronomy, KU Leuven, Celestijnenlaan 200D, B-3001 Leuven, Belgium*
[2]*Departamento de Física, Universidade Federal de Pernambuco, Cidade Universitária, 50670-901 Recife, Pernambuco, Brazil*

(Received 17 March 2020; revised 10 July 2020; accepted 13 July 2020; published 7 August 2020)

We study numerically the fractional Shapiro step response in low-frequency driven Josephson junctions which have a nonsinusoidal current-phase relation. We perform this study within the resistively shunted Josephson junction model. We demonstrate that fractional steps, as a fingerprint of a skewed current phase relation, will manifest themselves only for higher values of the reduced frequency. We compare the theoretical observations with experimental measurements in an anisotropic Josephson junction array containing over 500 superconductor-normal-superconductor junctions having a skewed current phase relation. We demonstrate that changing the critical current by applying a magnetic field is a robust method to modify the reduced frequency over a broad range of values. The presence of fractional Shapiro steps at high values of the reduced frequency directly confirm the theoretical results.

DOI: 10.1103/PhysRevB.102.054507

I. INTRODUCTION

The potential of Josephson junctions for applications in the terahertz range stems from the second Josephson relation, $\frac{d\varphi}{dt} = \frac{2e}{\hbar}V$. Due to the smallness of the flux quantum ($\Phi_0^{-1} = \frac{2e}{h} \approx 0.5\,\mathrm{GHz}/\mu\mathrm{V}$), this relation reflects that a small variation of the voltage drop V over a junction leads to a fast variation of the phase difference $\varphi(t)$ between the two superconducting electrodes [1]. Moreover, a driven Josephson junction (JJ) has the ability to have a resonant or phase-locked response when subjected to a high-frequency radiation field of frequency ν_{ac} [2]. This resonant response manifests itself as constant-voltage plateaus, so-called Shapiro steps, in the V-I characteristics of the junction at voltage values

$$V_{\frac{n}{q}} = \frac{n}{q}\Phi_0\nu_{ac}. \tag{1}$$

These voltages depend only on a fundamental constant, the flux quantum Φ_0, and the driving frequency ν_{ac}. Further, $q \in \mathbb{N}_0$, $n \in \mathbb{Z}$, and the qth ($\neq n$) fractional step originates from the phase-locked response with the qth harmonic in the current-phase relation ($C\Phi R$) [3–5],

$$I_s(\varphi) = I_c \sum_{q=1}^{\infty} b_q \sin(q\varphi), \tag{2}$$

where $I_c \equiv \max[I_s(\varphi)]$ is the critical current of the junction. The harmonic content of $C\Phi R$ is determined not only by the nature and geometry of the Josephson junction but also by temperature, the transport parameters of the superconducting banks, and the properties of the JJ interfaces [6–8].

In a recent work [9], the phase-locked response was measured on anisotropic Josephson junction arrays (JJAs). It was demonstrated that an anisotropic JJA shows single-junction behavior, free of collective effects [10–13]. The array geometry provides a giant Shapiro response and high device critical currents, making the measurement of the Shapiro response easily accessible even for drive frequencies as low as $\nu_{ac} = 50$ MHz. As the $C\Phi R$ becomes nonsinusoidal for a transparent superconductor-normal-superconductor (SNS) junction when approaching $T = 0$, this system provides a perfect playground for investigating the nonlinear resonant response of a JJ with a $C\Phi R$ containing higher-harmonic terms, as described by Eq. (2) [7,14]. The presence of giant fractional Shapiro steps, under certain strict experimental conditions, is direct evidence of the nonsinusoidal $C\Phi R$. Nevertheless, a detailed interpretation of such experiments is complicated by the strong nonlinear nature of the Josephson junction's response to an ac excitation. In order to identify the experimental conditions needed to observe the impact of higher-order modes in $C\Phi R$ on the Shapiro response, a direct comparison with detailed theoretical modeling is required.

In this paper, we will extend the work of Russer [15] and Likharev [16,17] discussing the Shapiro response of a JJ which has a sinusoidal $C\Phi R$ ($b_q = 0$ for $q > 1$) to the case of JJs with a $C\Phi R$ containing higher-harmonic terms. We will consider only the limit of overdamped JJs characterized by a Stewart-McCumber parameter [18,19], $\beta \ll 1$, as described within a resistively shunted Josephson junction model (RSJ model). This limit is appropriate for a quantitative description of externally shunted junctions of any type and for a qualitative description of (unshunted) weak links [16]. For a discussion regarding the intermediate damped and underdamped case $\beta \gg 1$, we refer to Refs. [16,20–25]. In addition, we perform transport measurements on an anisotropic JJA containing over 500 SNS junctions. The measurements are performed at 400 mK temperature to ensure a skewed current-phase relation [9]. These results show good qualitative correspondence with

*raes.bart@kuleuven.be
†These authors contributed equally to this work.

the model. The obtained insights can be used to define the experimental conditions enabling the observation of fractional Shapiro steps.

II. THE CURRENT-BIASED SHAPIRO MAP

A Shapiro map, which traces the width of the Shapiro plateaus as a function of the ac and dc drive of the system, is a very powerful tool to investigate the harmonic content of the $C\Phi R$ in a variety of weak links. Examples include weak links, where the coupling between the superconducting banks is established by a normal metal; a topological insulator; and graphene [26–30]. As such, we will focus our attention on these types of experiments. In case the drive has a voltage nature, $v_{bias} = v_{dc} + v_{ac}\cos(\omega_{ac}t)$, with $\omega_{ac} = 2\pi\nu_{ac}$, the current contains a dc current component when $v_{dc} = V_{\frac{n}{q}}$, where $n \in \mathbb{Z}, q \in \mathbb{N}_0$. The dc component can be obtained analytically in closed form and is given by (see the Supplemental Material [31])

$$I_0 = I_c \sum_{q=1}^{\infty} b_q J_0\left(q\frac{2e}{\hbar\omega_{ac}}v_{ac}\right)\sin(q\triangle\varphi_0), \quad n = 0, \tag{3a}$$

$$I_{\frac{n}{q}} = I_c \sum_{q'=1}^{\infty} b_{q'}(-1)^{q'n} J_{q'n}\left(q'\frac{2e}{\hbar\omega_{ac}}v_{ac}\right)\sin(q'\triangle\varphi_0) \quad \text{for integer steps, } n \in \mathbb{Z}_0, q = 1, \tag{3b}$$

$$I_{\frac{n}{q}} = I_c \sum_{q'=1}^{\infty} b_{q'q}(-1)^{q'n} J_{q'n}\left(qq'\frac{2e}{\hbar\omega_{ac}}v_{ac}\right)\sin(qq'\triangle\varphi_0) \quad \text{for fractional steps, } n \in \mathbb{Z}_0, q \in \mathbb{N} > 1, \mathrm{mod}(n, q) \neq 0, \tag{3c}$$

where J_n is the nth-order Bessel function of the first kind, $\triangle\varphi_0$ is the initial phase difference [8,32], and the fractional step number $\frac{n}{q}$ is always considered to be written in the lowest terms. Note that this solution has an oscillatory dependence on the amplitude of the applied ac voltage (as it appears inside of the Bessel function), while it is independent of the particular value of I_c or b_q.

In the majority of experimental arrangements, no special measures are employed to provide matching. As such, the impedance of the environment is larger than the characteristic impedance of the JJ, and the driving source acts as a current source. For such a current-biased system, $i_{bias} = i_{dc} + i_{ac}\cos(\omega_{ac}t)$, where $i_k = I_k/I_c$ (with $k = \mathrm{ac}, \mathrm{dc}$) is the reduced current, the Shapiro map can be obtained only numerically. It is well established that in the case of a sinusoidal $C\Phi R$ only integer Shapiro steps appear [16] (see the Supplemental Material [31]). In general, the current width of the nth-integer Shapiro step depends in a nontrivial way on the reduced frequency [15–17]:

$$\Omega = \frac{\Phi_0 \nu_{ac}}{2\pi R I_c}. \tag{4}$$

This reduced frequency is a measure of the ratio of the magnitude of the minimum impedance of the Josephson junction and the magnitude of the impedance of the resistive channel [8,16]. Moreover, in the current-biased case the Shapiro map is independent of the initial phase difference over the junction. To investigate the impact of higher harmonics in the $C\Phi R$ on the Shapiro step response, we integrate numerically the overdamped RSJ equation of motion [9–12]

$$\frac{\hbar}{2eR}\frac{d\varphi}{dt} = I_{dc} + I_{ac}\cos\omega_{ac}t - I_s(\varphi, \ell) \tag{5}$$

for a current-biased noise-free junction, characterized by $C\Phi R$ given by

$$I_s(\varphi, \ell) = I_c \sin\left(\varphi - \ell\frac{I_s}{I_c}\right), \tag{6}$$

where $I_c = \max(|I_s|)$ is the critical current of the junction. The parameter ℓ is given by

$$\ell = I_c\left(\frac{dI_s}{d\varphi}\right)_{\pi}^{-1} + 1, \tag{7}$$

which has a simple geometrical interpretation and determines the level of skewness of $C\Phi R$ [6,7]. Equation (6) is only an approximation of the real $C\Phi R$ [Eq. (2)]; however, it captures the main aspects using only two parameters. The upper and lower limits of each Shapiro step were determined numerically by carefully sweeping the dc current for given values of the reduced frequency Ω and ac amplitude i_{ac} within a bisection algorithm. For each set of values of i_{dc}, i_{ac}, and Ω, the full equation was integrated using the fourth-order Runge-Kutta method over typically 2×10^7 time steps of size $h = 0.01t_0$, where t_0 is the Josephson time.

A. Impact of the reduced frequency for an unskewed $C\Phi R$

As a first step we construct the Shapiro map for an unskewed $C\Phi R$ and explore the impact of the reduced frequency. Some representative Shapiro step diagrams for the sinusoidal case [$\ell = \mathbf{0}$ ($b_q = 0, q > 1$)] are shown in Fig. 1(a). They present the dependence of the reduced Shapiro current step widths, $\Delta i_n = \Delta I_n/I_c$, on the reduced frequency. These diagrams show the reduced dc current drive i_{dc} on the x axis and the reduced ac current drive i_{ac} on the y axis. Regions in this parameter space where phase-locked solutions (Shapiro steps) were identified are colored; regions where none were identified remain blank.

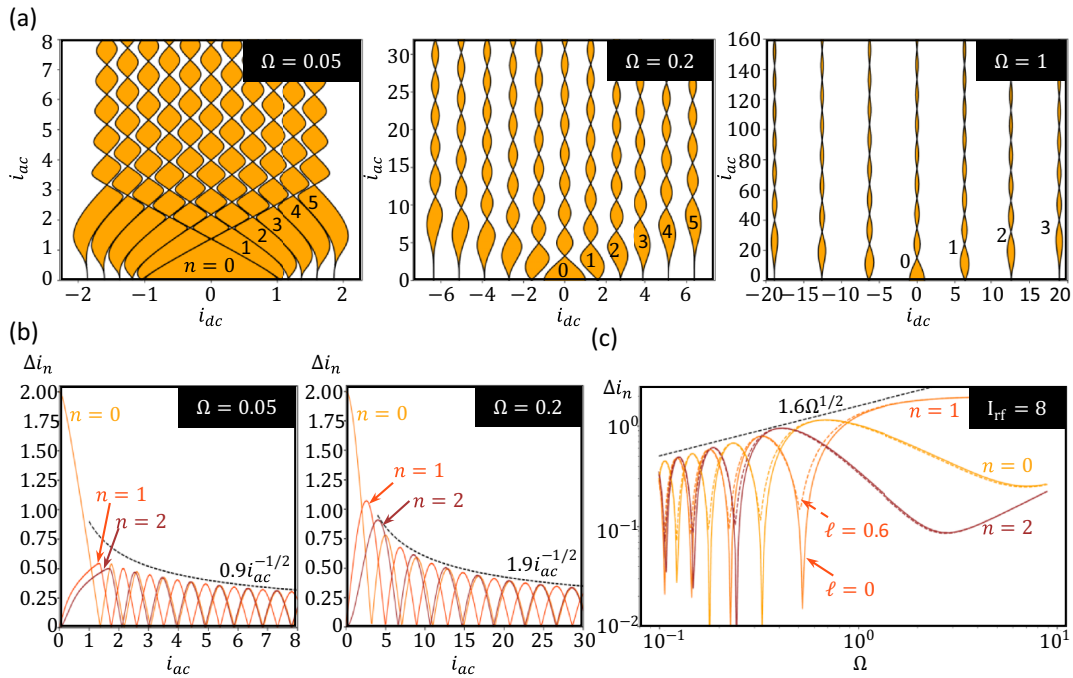

FIG. 1. (a) Shapiro step diagrams for the sinusoidal case, $\ell = 0$, and three different reduced frequencies, $\Omega = 0.05, 0.2, 1$. In these Shapiro step diagrams orange fills delimited by black lines correspond to integer steps; fractional steps could not be identified for $\ell = 0$. The numbers in the Shapiro map indicate the integer step number n. (b) The reduced current step width of the first three integer Shapiro steps Δi_n ($n = 0, 1, 2$) as a function of the ac current amplitude i_{ac} for two different reduced frequencies $\Omega = 0.05, 0.2$. The dashed black lines illustrate that the maximum of the width of steps scales as $i_{ac}^{-1/2}$. (c) The width of the first three integer Shapiro steps Δi_n ($n = 0, 1, 2$) as a function of reduced frequency Ω for a fixed reduced ac current amplitude $i_{ac} = 8$ as a log-log plot. Solid lines are for $\ell = 0$, while dashed lines correspond to $\ell = 0.6$. The dashed black line indicates that the maximum of the width of steps scales as $\sqrt{\Omega}$.

The Shapiro step diagrams shown in Fig. 1(a) contain only signatures of integer Shapiro steps ($q = 1$). The corresponding amplitude and frequency dependence of the reduced current step widths, $\Delta i_n = \Delta I_n / I_c$, of the first $n = 0, 1, 2$ steps are shown in Figs. 1(b) and 1(c), respectively. The dependence of the integer ($q = 1$) reduced current step widths on the reduced ac amplitude and reduced frequency follows a Bessel-like dependence over a wide range of amplitudes and frequencies:

$$\Delta i_n \sim J_n\left(\frac{i_{ac}}{\Omega}\right), \qquad n \in \mathbb{Z},\ q = 1. \tag{8}$$

It is remarkable that, for a wide range of values for the reduced frequency, the Bessel-like dependence, as obtained for the voltage-biased case [Eq. (3)], is qualitatively preserved for the current-biased junctions. This was already observed by Likharev [16], who showed that the Bessel-like dependence persists if one of the following conditions is fulfilled: $\Omega \geqslant 1$, $i_{ac}\Omega \geqslant 1$, or $n\Omega^3 \geqslant 1$. According to the properties of the Bessel functions of the first kind, $J_n(z)$ increases first as z^n and reaches a maximum value of $0.675 n^{-1/3}$ at $z \sim n$. For large values of z and any value of n $J_n(z)$ slowly decrease, oscillating with a period $\triangle z \sim 2\pi$, under an envelope as $\sqrt{2/(\pi z)}$. This asymptotic behavior, with $z = i_{ac}/\Omega$, is indicated by the black dashed lines in Figs. 1(b) and 1(c).

Only in the case of low ac current amplitudes, low reduced frequencies, and low step numbers does the step size not follow the Bessel-like dependence. In this case [Fig. 1(b), left panel, $\Omega = 0.05$], Δi_0 decreases nearly linearly with increasing ac current amplitude. In addition, the widths of the first and second Shapiro steps $\Delta i_{1,2}$ are roughly equal and increase as $\sqrt{i_{ac}}$ [33].

Since the impact of the higher harmonics of $C\Phi R$ is expected to introduce fractional steps, a sufficiently large spacing is required between the consecutive integer Shapiro steps. For the range of parameters where Eq. (8) is valid, the dc current spacing between two consecutive Shapiro steps (white zones in Fig. 1) is proportional to (see the Supplemental Material [31])

$$\Delta I_{dc}^{\text{nosteps}} = \frac{\Phi_0 \nu_{ac}}{R} - I_c\left(\frac{\Phi_0 \nu_{ac}}{2\pi I_{ac} R}\right)^{1/2} \tag{9a}$$

$$= \Omega I_c\left[2\pi - \left(\frac{I_c}{I_{ac}\Omega}\right)^{1/2}\right]. \tag{9b}$$

Consequently, the range of dc currents ΔI_{dc} between two consecutive Shapiro steps (orange zones) increases with reduced frequency for a fixed critical current I_c and ac drive amplitude I_{ac}.

B. Shapiro map for a skewed $C\Phi R$

Figure 2(a) shows Shapiro maps for the case $\ell \neq \mathbf{0}$ for a fixed reduced frequency $\Omega = 0.2$ and three different levels of skewness, $\ell = 0.2, 0.6, 0.8$. The color code in Fig. 2(a) distinguishes between the different Shapiro regions, with white

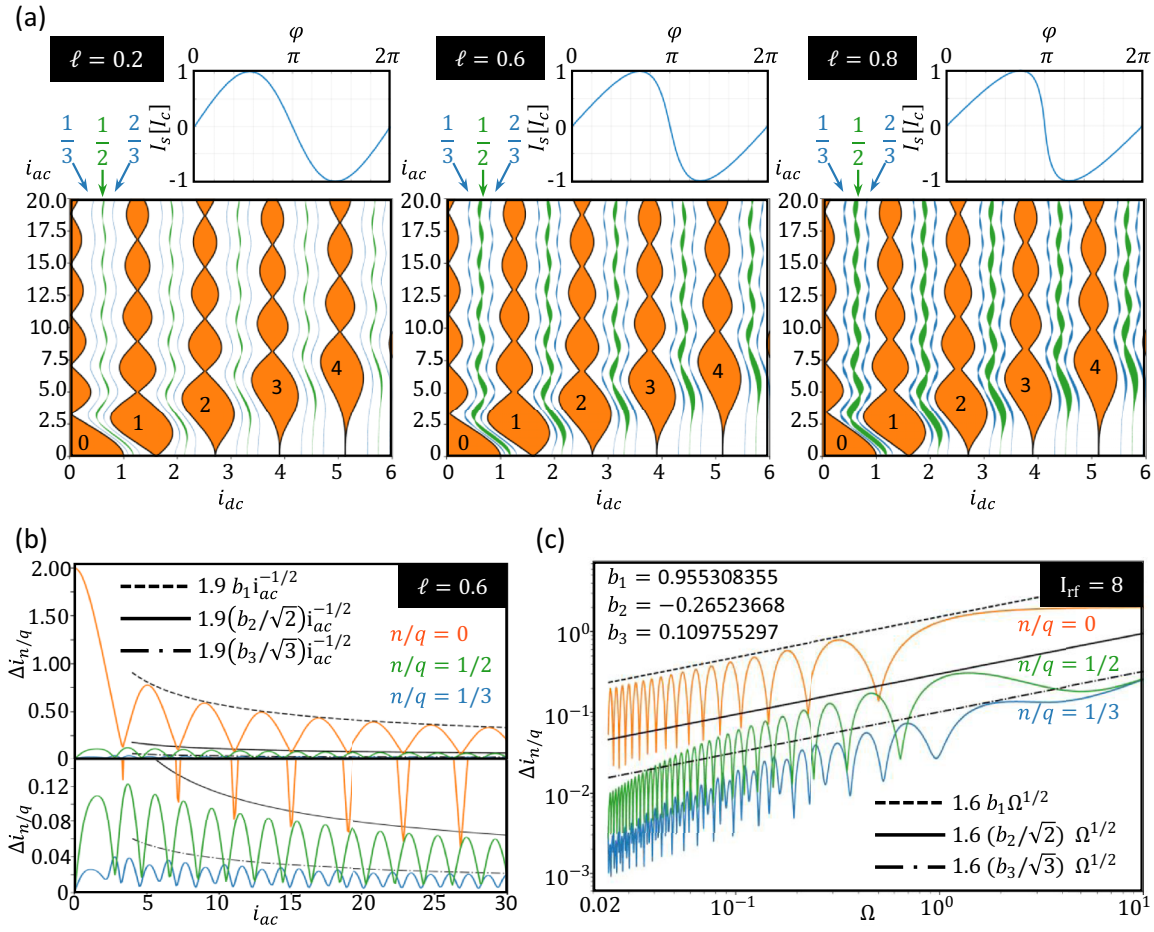

FIG. 2. (a) Shapiro step diagrams for a fixed reduced frequency $\Omega = 0.2$ and three different levels of skewness, $\ell = 0.2, 0.6, 0.8$. In these Shapiro step diagrams orange fills delimited by black lines correspond to integer steps, while green and blue fills correspond to the $q = 2$ and $q = 3$ fractional steps, respectively. Higher-order fractional steps, $q > 3$, are not indicated. The numbers above and in the Shapiro map indicate the step number n/q. Additionally, we show the $C\Phi R$ for each value of the skewness parameter. (b) The width of the zeroth, $(1/2)$th and $(1/3)$th Shapiro steps $\Delta i_{n/q}$ as a function of the reduced ac current amplitude i_{ac} for a reduced frequency $\Omega = 0.2$ and $\ell = 0.6$. The black lines illustrate that the maximum of the width of the (n/q)th step scales as $b_q q^{-1/2} i_{ac}^{-1/2}$. (c) The width of the zeroth, $(1/2)$th, and $(1/3)$th Shapiro steps $\Delta i_{n/q}$ as a function of reduced frequency Ω for a fixed reduced ac current amplitude $i_{ac} = 8$ as a log-log plot. The black lines illustrate that the maximum of the width of the (n/q)th step scales as $b_q q^{-1/2}\sqrt{\Omega}$.

meaning no phase-locked solutions were identified, orange for integer steps, and other colors for the fractional steps. It is clear all three Shapiro maps contain both integer ($q = 1$) and fractional Shapiro steps. Only the first $\Delta i_{\frac{n}{q}}$, with $q = 1, 2, 3$, steps are shown in the Shapiro map. Higher-order fractional steps, $q > 3$, are not indicated. The dependence of the step widths on the reduced ac drive amplitude and the reduced frequency for $\ell = 0.6$ are shown in Figs. 2(b) and 2(c), respectively.

When a current-biased junction has a skewed $C\Phi R$, the Bessel-like dependence of the reduced fractional step widths on the reduced ac amplitude and reduced frequency, as obtained for the voltage-biased case, is also qualitatively preserved for a broad range of drive parameters. It is given in first-order approximation by

$$\Delta i_{\frac{n}{q}} \sim b_q J_n\left(q\frac{i_{ac}}{\Omega}\right) \tag{10}$$

for $n \in \mathbb{Z}_0$, $q \in \mathbb{N} > 1$, and $\mathrm{mod}(n, q) \neq 0$. The dependence of the reduced fractional step widths on the reduced ac amplitude and reduced frequency, as formulated by Eq. (10), is confirmed by several observations:

(i) For each oscillation of the integer steps ($q = 1$, $n = 0, 1, \ldots$), in a plot of the reduced step width versus the reduced ac amplitude [Fig. 2(b)] or frequency [Fig. 2(c)], there are q local minima for the fractional steps ($q = 2, 3, 4, \ldots$). This is qualitatively similar to the voltage bias case, Eq. (3c), where the resonance condition would lead to Bessel-like oscillations with a period q times smaller than that of the fundamental ($n = 0$) resonance.

(ii) The black lines in Figs. 2(b) and 2(c) indicate that the dependence of the (n/q)th step width on the reduced ac current amplitude i_{ac} and reduced frequency Ω qualitatively follows the expected Bessel-like dependence [Eq. (10)] when i_{ac} and Ω are sufficiently large and if we consider that the b_q components decrease rapidly with increasing q. For

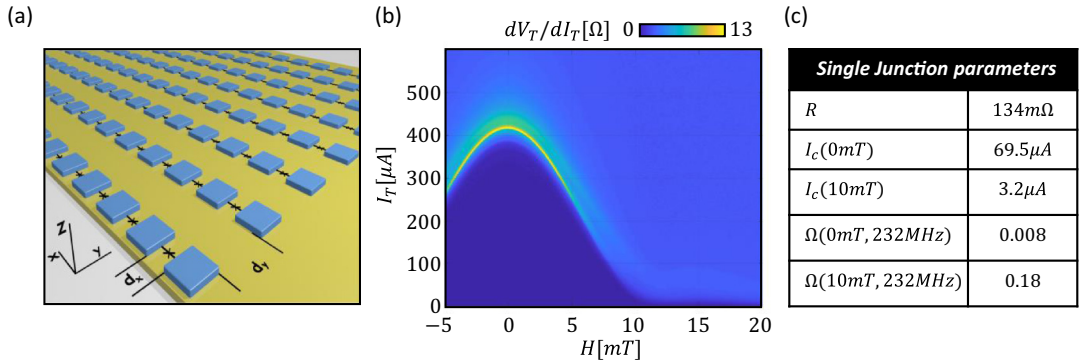

FIG. 3. (a) A schematic illustration of the superconductor-normal metal (S-N) hybrid device studied in this work. (b) The magnetic field H and dc current I_T dependence of the differential resistance dV_T/dI_T of the anisotropic JJA at $T = 400$ mK when no high-frequency ac excitation is applied. The differential resistance is measured by a standard lock-in technique. (c) Single-junction parameters, including the value of the resistive shunt, the critical current, and reduced frequency.

$\ell = 0.6$, the first three corresponding Fourier coefficients b_q are indicated in Fig. 2(c).

(iii) The (n/q)th step width scales with the value of the corresponding qth Fourier component b_q.

The asymptotic dependence of the maximum fractional current step widths on the reduced frequency and amplitude approximately follows a Bessel-like dependence, as discussed above. The oscillatory behavior of the fractional steps, however, is more irregular. This is shown in the bottom panel of Fig. 2(b), and it is qualitatively similar to the voltage bias case, where at the qth fractional resonance condition, the different $(k \times q)$th harmonics, with $k \in \mathbb{N}_0$, also contribute to the step width [see Eq. (3c)].

The higher-harmonic content in the $C\Phi R$ also has an impact on the integer step widths. To illustrate this we show Fig. 1(c), which displays the variation of the first three integer step widths, $n = 0, 1, 2$, and $q = 1$, with reduced frequency for $\ell = 0.6$ (dashed lines) and $\ell = 0$ (solid lines). By comparing the integer Shapiro steps widths in the Shapiro maps in Figs. 1(a) and 2(a), one can observe that whereas the reduced Shapiro current step widths disappear for particular values of i_{ac}, for the sinusoidal case, the Shapiro current step widths remain finite for all i_{ac} for a skewed $C\Phi R$. This is again qualitatively similar to the voltage-biased case, where the different $(k \times n)$th harmonics, with $k \in \mathbb{N}_0$, also contribute to the integer step widths [see Eq. (3b)].

III. EXPERIMENTAL RESULTS

A. Device characteristics

We compare the above theoretical observations with measurements on a highly anisotropic Josephson junction array containing over 500 SNS junctions. The array layout is schematically shown in Fig. 3(a). The array consist of $N_x \times N_y = 93 \times 63$ MoGe squares on top of a 40-nm-thick gold film. The metallic base layer couples the different superconducting islands through the proximity effect, resulting in a two-dimensional proximity-induced SNS Josephson junction array [34]. The squares have a size of 500×500 nm^2 and are $d_x = 250$ nm separated along the current direction (x direction), while the separation perpendicular to the current direction is $d_y = 1$ μm. This results in a highly anisotropic array with $\eta = d_y/d_x = 4$.

As shown in Ref. [9], which discusses a similar sample, the high anisotropy of the array ensures that the array shows single-junction behavior, free of collective effects in the array [10–13]. Moreover, the large number of junctions results in a giant Shapiro response and high device critical currents. It is well known and also discussed in Ref. [9] that for a prototypical SNS junction the $C\Phi R$ becomes forwardly skewed at low temperatures [14]. By measuring the temperature dependence of the critical current at zero field on similar samples [9], we can estimate the normal-metal coherence length to be $\xi_N(T_c) \sim 45$–55 nm. Using this estimation of ξ_N and considering the geometrical length of the link, $d_x = 250$ nm, we apply Likharev's equilibrium description of a hard-boundary SNS junction. This allows us to estimate the skewness parameter $\ell \sim 0.5$ at $T = 400$ mK.

The field dependence of the critical current is shown in Fig. 3(b). It exhibits the typical Fraunhofer-like dependence illustrative of an extended weak link. This confirms that the whole array behaves as a single Josephson junction. Note that the particular field dependence of the critical current is determined by the geometry of the normal metallic weak link and can deviate from the ideal Fraunhofer dependence [35]. In Fig. 3(c) we show the estimated values for the critical current and the value of the resistive shunt for a single junction at $H = 0$ mT and $H = 10$ mT, together with the corresponding values of the reduced frequency. The relation between the current and voltage over a single junction (no subscript or superscript T) and the current and voltage over the whole array (subscript or superscript T) is given through the relations $I_T = N_x I$ and $V_T = (N_y - 1)V$.

B. The dependence of the Shapiro response on the reduced frequency

Changing the reduced frequency Ω can be done in two different ways: by changing the ac frequency of the drive, ν_{ac} or by changing the critical current I_c. Figures 4(a) and 4(b) show the experimentally obtained dependence of the Shapiro steps as a function of the radio frequency ν_{ac} and as

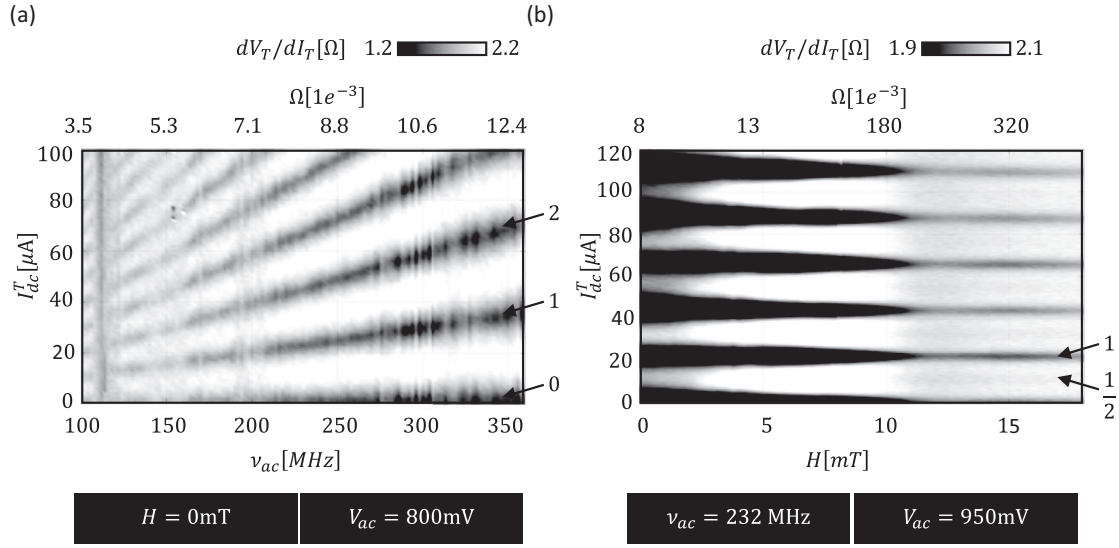

FIG. 4. (a) The experimentally measured frequency dependence of the Shapiro steps for a fixed rf excitation amplitude of $V_{ac} = 800$ mV at $T = 0.4$ K. Shapiro steps are clearly reflected in the map, as the zones of low differential resistance (black). The numbers on the side indicate the Shapiro step number. (b) The experimentally measured field dependence of the Shapiro response is shown as a contour map of the differential resistance as a function of the applied magnetic field and applied dc current for $T = 0.4$ K. The rf excitation parameters are $\nu_{ac} = 232$, MHz and $V_{rf} = 950$ mV. The numbers on the side indicate the Shapiro step number.

a function of the applied magnetic field H at a fixed drive amplitude, respectively. Shapiro steps are reflected as (black) zones of low differential resistance. The estimated value of the corresponding reduced frequency is shown on the top axis for both cases. The rf excitation is experimentally applied by a function generator. This means that the conversion between the applied rf voltage and the transmitted rf current is *a priori* unknown and can depend strongly on the rf frequency. However, in both cases the drive current $I_{ac} \gg I_c$.

In Fig. 4(a), we show the dependence of the Shapiro steps when changing the drive frequency in the range $\nu_{ac} =$ 100–300 MHz at zero applied magnetic field and for a fixed large drive amplitude of $V_{ac} = 800$ mV. The data show signatures of integer Shapiro steps only in this range of Ω and for this particular drive amplitude. In accordance with theory, we observe that the distance between the steps increases linearly with Ω and that the current width of the Shapiro steps, which scales with the value of the minima in the differential resistance as $\Delta I_n \sim (dV_T/dI_T)^{-1}$, increases with Ω. However, we did not observe a clear oscillatory dependence of the step widths on the drive frequency. This could be explained by smearing of the Shapiro steps due to unavoidable disorder in the Josephson junction array and thermal fluctuations [36].

Note that experimentally, continuously changing the drive frequency in the range of interest (megahertz to gigahertz) is challenging due to the typically complex frequency dependence of the transfer function of the excitation system. Moreover, this frequency tuning allows us to change Ω over only a small range. Additionally, high frequencies can have an impact on the $C\Phi R$ itself [as they can change (and control) the Andreev bound-state spectrum occupancy] [14,37]. Because of these considerations, methods that allow studying the $C\Phi R$ in a broad frequency range are highly relevant [38].

In Fig. 4(b), we alternatively change the reduced frequency by changing the critical current through exploiting its Fraunhofer-like magnetic field dependence. In this case the reduced frequency Ω changes by orders of magnitude. The comparison with theory (Figs. 1 and 2) is not straightforward in this case, as the Shapiro maps and the dependences of the Shapiro step widths on the ac amplitude and reduced frequency are discussed in terms of reduced units. However, using the asymptotic limits of the Bessel function (valid for $i_{ac}/\Omega \gg 1$), we can derive that the magnitude of the nth integer current step width scales with the critical current as

$$\Delta I_n \sim I_c \left(\frac{i_{ac}}{\Omega}\right)^{-\frac{1}{2}} \sim I_c \left(\frac{\Phi_0 \nu_{ac}}{2\pi R I_{ac}}\right)^{\frac{1}{2}}. \tag{11}$$

As the step widths scale linearly with I_c, they should follow a Fraunhofer-like dependence on the applied magnetic field, as can be observed in Fig. 4(b). Only for $H > 9$ mT do we observe fractional Shapiro steps, which corresponds to the observations in Sec. II and Eq. (9). Only when I_c becomes sufficiently small (meaning for increasing Ω) does the dc current range where no integer Shapiro steps can be identified increase, leaving room for the manifestation of fractional Shapiro steps. As indicated in Sec. II, the ratio of the current width of the (n/q)th fractional steps and the nth integer steps scales with the ratio of the Fourier components as $b_q/(\sqrt{q}b_n)$, which for $\ell = 0.5$ is about 0.20 (for $n = 1$, $q = 2$) and explains the lower intensity of the half fractional Shapiro steps in comparison to the integer steps. Higher-order fractional steps, $q > 2$, could not be identified.

C. The dependence of the Shapiro response on the drive amplitude

Figure 5 shows two experimentally obtained Shapiro maps, both obtained at a fixed frequency of $\nu_{ac} = 232$ MHz, but at different low magnetic field values, $H = 0$ mT and

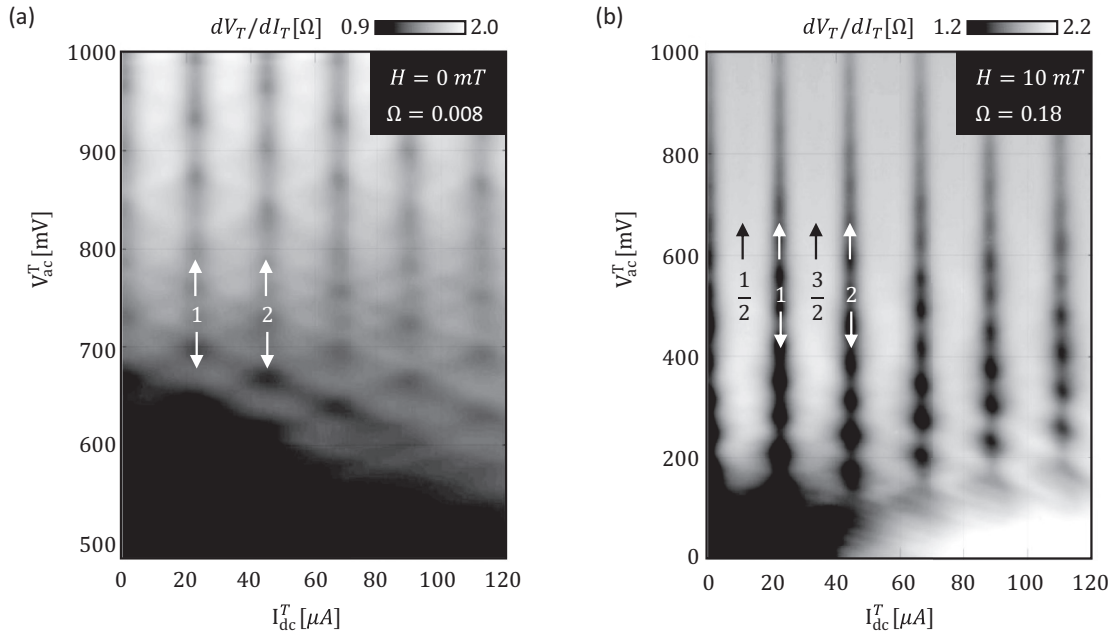

FIG. 5. (a) The evolution of the Shapiro steps as a function of rf amplitude in a so-called Shapiro map. In particular the experimentally obtained dependence of the differential resistance dV_T/dI_T as a function of the ac drive amplitude and dc current for a fixed radio frequency, $\nu_{ac} = 232$ MHz at $T = 400$ mK and zero field is shown. (b) Similar data as for (a). The experimentally obtained dependence of the differential resistance dV_T/dI_T as a function of the ac drive amplitude and dc current for a fixed radio frequency $\nu_{ac} = 232$ MHz at $T = 400$ mK and $H = 10$ mT is shown.

$H = 10$ mT, corresponding to $\Omega(0\,\text{mT}) = 0.008$ and $\Omega(10\,\text{mT}) = 0.18$, respectively [see Fig. 3(c)]. Note that it is difficult to pick a color scale that shows the Shapiro steps clearly over the whole amplitude range as the offset on which the Shapiro steps live changes with rf amplitude. As such, we show some additional cross sections for both cases in Figs. 6(a) and 6(b).

For $H = 10$ mT (corresponding to $\Omega = 0.18$ and $I_c = 3.2\,\mu$A), it is clear that the Shapiro step widths decrease with increasing ac drive amplitude [see Eq. (11)]. Simultaneously, the dc current range where no integer Shapiro steps can be identified increases [see Eq. (9)]. Only for drive amplitudes exceeding $V_{rf} > 650$ mV can we observe the $n \times (1/2)$th steps, with $n \in \mathbb{N}_0$ and $\text{mod}(n, q) \neq 0$. This is more clearly shown in Fig. 6(b). Note that as discussed before, the ratio of the current width of the (n/q)th fractional steps and the nth integer steps scales with the ratio of the Fourier components as $b_q/(\sqrt{q}b_n)$, which for $\ell = 0.5$ is about 0.20 (for $n = 1$,

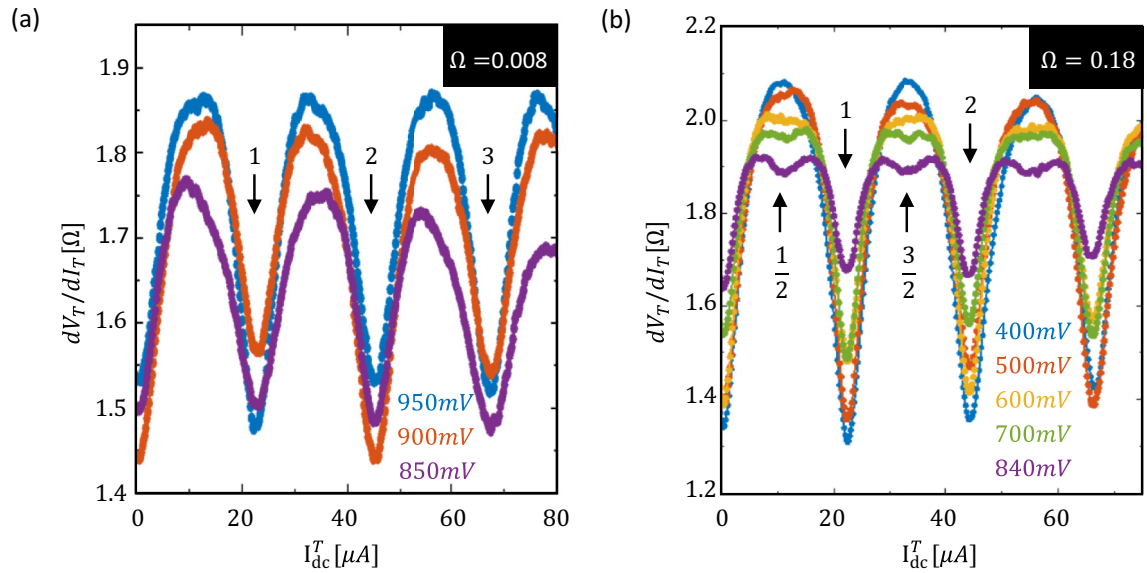

FIG. 6. (a) Some selected dV_T/dI_T vs I_{dc} curves for different ac excitation amplitudes as extracted from Fig. 5(a). (b) Some selected dV_T/dI_T vs I_{dc} curves for different ac excitation amplitudes as extracted from Fig. 5(b).

$q = 2$). This explains the lower intensity of the half fractional Shapiro steps in comparison to the integer steps. Higher-order fractional steps, $q > 2$, could not be identified in the map.

For $H = 0$ mT (corresponding to $\Omega = 0.008$ and $I_c = 69.5\,\mu$A), no fractional steps can be observed within the range of experimentally accessible ac drive amplitudes. The low-field condition is unfavorable to observe fractional steps at this particular ac drive frequency. Compared to the $H = 10$ mT case, the explored ac drive range reveals only the first five integer Shapiro steps, whereas in the $H = 10$ mT case more than 13 steps can be identified. As such, the amplitude dependence of the integer Shapiro steps shown in Fig. 6(a) does not reflect the overall asymptotic dependence of the Bessel function in Eq. (8) but is governed by the details of the current step width oscillation of only a few Shapiro steps.

IV. CONCLUSIONS

In this work we extended the work of Russer [15] and Likharev [16,17] discussing the Shapiro response of a JJ with a sinusoidal $C\Phi R$ ($b_q = 0$ for $q > 1$) to the case of JJs with a $C\Phi R$ containing higher-harmonic terms. We limited the discussion to the case of overdamped JJs characterized by a Stewart-McCumber parameter, $\beta \ll 1$, as described within a resistively shunted Josephson junction model. By numerically calculating the Shapiro response, we showed that the response of a Josephson junction with a skewed $C\Phi R$ is qualitatively similar to the voltage-biased solution for a broad range of parameters and that a higher value of Ω promotes the observation of fractional Shapiro steps. A qualitative comparison with experimentally obtained Shapiro responses on a highly anisotropic Josephson junction array was presented in Sec. III. As established in Ref. [9], the SNS junctions in this JJA have a skewed $C\Phi R$ at low temperatures, with skewness parameter $\ell = 0.5$ at $T = 400$ mK. We compared the measured dependence of the Shapiro response on the reduced frequency $\Omega(I_c, \nu_{ac})$ when changing I_c or ν_{ac} independently. These results indicate that (i) a complete picture is required in order to explore the details of $C\Phi R$ through measurements of the Shapiro response and (ii) a powerful method to obtain a high reduced frequency (which favors observation of fractional Shapiro steps as shown in Sec. II) while keeping the drive frequency low is to change the critical current using a magnetic field. In order to obtain a more accurate correspondence between data and experiment, the unavoidable disorder in the Josephson junction array due to sample fabrication and temperature fluctuations has to be taken into account.

ACKNOWLEDGMENTS

B.R., R.P., H.D., and J.V.d.V. acknowledge support from the Flemish Science Foundation (Grant No. G0B5315N). This work has been supported by the COST action NanoCoHybri (CA16218). This work was supported by the Brazilian Agencies Fundação de Amparo a Ciência e Tecnologia do Estado de Pernambuco (FACEPE, under Grant No. APQ-0198-1.05/14), Coordenação de Aperfeiçoamento de Pessoal de Nível Superior (CAPES), and Conselho Nacional de Desenvolvimento Científico e Tecnológico (CNPq).

[1] B. Josephson, Phys. Lett. **1**, 251 (1962).
[2] S. Shapiro, Phys. Rev. Lett. **11**, 80 (1963).
[3] P. Dubos, H. Courtois, O. Buisson, and B. Pannetier, Phys. Rev. Lett. **87**, 206801 (2001).
[4] D. Cassel, G. Pickartz, M. Siegel, E. Goldobin, H. Kohlstedt, A. Brinkman, A. Golubov, M. Kupriyanov, and H. Rogalla, Phys. C (Amsterdam, Neth.) **350**, 276 (2001).
[5] I. N. Askerzade, Low Temp. Phys. **41**, 241 (2015).
[6] A. A. Golubov, M. Y. Kupriyanov, and E. Il'ichev, Rev. Mod. Phys. **76**, 411 (2004).
[7] K. K. Likharev, Rev. Mod. Phys. **51**, 101 (1979).
[8] F. Tafuri, *Fundamentals and Frontiers of the Josephson Effect*, 1st ed., Vol. 286 (Springer International Publishing, Switzerland, 2019).
[9] R. Panghotra, B. Raes, C. C. de Souza Silva, I. Cools, W. Keijers, J. E. Scheerder, V. V. Moshchalkov, and J. Van de Vondel, Commun. Phys. **3**, 53 (2020).
[10] J. S. Chung, K. H. Lee, and D. Stroud, Phys. Rev. B **40**, 6570 (1989).
[11] J. U. Free, S. P. Benz, M. S. Rzchowski, M. Tinkham, C. J. Lobb, and M. Octavio, Phys. Rev. B **41**, 7267 (1990).
[12] M. Octavio, J. U. Free, S. P. Benz, R. S. Newrock, D. B. Mast, and C. J. Lobb, Phys. Rev. B **44**, 4601 (1991).
[13] I. R. Rahmonov, J. Tekić, P. Mali, A. Irie, and Y. M. Shukrinov, Phys. Rev. B **101**, 024512 (2020).
[14] M. Fuechsle, J. Bentner, D. A. Ryndyk, M. Reinwald, W. Wegscheider, and C. Strunk, Phys. Rev. Lett. **102**, 127001 (2009).
[15] P. Russer, J. Appl. Phys. **43**, 2008 (1972).
[16] K. K. Likharev, *Dynamics of Josephson Junctions and Circuits* (Gordon and Breach, New York, 1988).
[17] K. K Likharev and V. K. Semenov, Radio Eng. Electron. Phys. **16**, 1917 (1971).
[18] W. Stewart, Appl. Phys. Lett. **12**, 277 (1968).
[19] D. E. McCumber, J. Appl. Phys. **39**, 3113 (1968).
[20] R. L. Kautz and R. Monaco, J. Appl. Phys. **57**, 875 (1985).
[21] R. L. Kautz, J. Appl. Phys. **62**, 198 (1987).
[22] V. Belykh, N. F. Pedersen, and O. Soerensen, Phys. Rev. B **16**, 4860 (1977).
[23] H.-D. Hahlbohm, A. Hoffmann, H. Lübbig, H. Luther, and S. Seeck, Phys. Status Solidi A **13**, 607 (1972).
[24] V. K. Kornev, T. Y. Karminskaya, Y. V. Kislinskii, P. V. Komissinki, K. Y. Constantinian, and G. A. Ovsyannikov, J. Phys.: Conf. Ser. **43**, 1105 (2006).
[25] V. Kornev, T. Karminskaya, Y. Kislinskii, P. Komissinki, K. Constantinian, and G. Ovsyannikov, Phys. C (Amsterdam, Neth.) **435**, 27 (2006).
[26] R. A. Snyder, C. J. Trimble, C. C. Rong, P. A. Folkes, P. J. Taylor, and J. R. Williams, Phys. Rev. Lett. **121**, 097701 (2018).

[27] K. Le Calvez, L. Veyrat, F. Gay, P. Plaindoux, C. B. Winkelmann, H. Courtois, and B. Sacépé, Commun. Phys. **2**, 4 (2019).

[28] G.-H. Lee, S. Kim, S.-H. Jhi, and H.-J. Lee, Nat. Commun. **6**, 6181 (2015).

[29] A. Assouline, C. Feuillet-Palma, N. Bergeal, T. Zhang, A. Mottaghizadeh, A. Zimmers, E. Lhuillier, M. Eddrie, P. Atkinson, M. Aprili, *et al.*, Nat. Commun. **10**, 126 (2019).

[30] M. Bae, R. Dinsmore, T. Aref, M. Brenner, and A. Bezryadin, Nano Lett. **9**, 1889 (2009).

[31] See Supplemental Material at http://link.aps.org/supplemental/10.1103/PhysRevB.102.054507 for (i) a derivation of the Shapiro step widths in the case of a voltage-biased Josephson junction having an anharmonic $C\Phi R$ and (ii) a derivation of the dc current width between two consecutive Shapiro steps.

[32] D. Langenberg, D. Scalapino, and B. Taylor, Proc. IEEE **54**, 560 (1966).

[33] M. Renne and D. Polder, Rev. Phys. Appl. **9**, 25 (1974).

[34] H. Meissner, Phys. Rev. **109**, 686 (1958).

[35] J. C. Cuevas and F. S. Bergeret, Phys. Rev. Lett. **99**, 217002 (2007).

[36] K. Ravindran, L. B. Gómez, R. R. Li, S. T. Herbert, P. Lukens, Y. Jun, S. Elhamri, R. S. Newrock, and D. B. Mast, Phys. Rev. B **53**, 5141 (1996).

[37] L. Bretheau, Ç. Girit, H. Pothier, D. Esteve, and C. Urbina, Nature (London) **499**, 312 (2013).

[38] B. Dassonneville, A. Murani, M. Ferrier, S. Guéron, and H. Bouchiat, Phys. Rev. B **97**, 184505 (2018).